Annals of Pharmacy Practice and Pharmacotherapy
ISSN: 3062-4436
2021, Volume 1, Page No: 80-93

Available online at: www.galaxypub.co/page/journals

Galaxy Publication

Galaxy Publication

Proteomic Discovery of Pharmacodynamic Biomarkers Using a Highly Efficient Protein Corona-Based Strategy

Hiroshi Tanaka[1], Akari Sato[1], Kenji Yamamoto[1]*

[1]Graduate School of Pharmaceutical Sciences, Kyoto University, Kyoto, Japan.

***E-mail** ✉ kenji.yamamoto@protonmail.com

Received: 26 January 2021; **Revised:** 28 April 2021; **Accepted:** 03 May 2021

ABSTRACT

Serum exhibits a highly complex composition, which poses challenges for discovering novel pharmacodynamic biomarkers through serum proteomics for disease prediction and diagnosis. Recent studies have shown that nanoparticles can effectively decrease the abundance of high-concentration proteins while enriching low-abundance proteins in serum. In this study, we synthesized silica-coated iron oxide nanoparticles and established a highly efficient and reproducible protein corona (PC)-based proteomic analysis approach to broaden the scope of serum proteome profiling. Using this PC-based strategy, we identified 1,070 proteins with a median coefficient of variation of 12.56%, representing twice the number of proteins detected by conventional direct digestion, along with enrichment in additional biological processes. We further applied this approach to detect pharmacodynamic biomarkers in a collagen-induced arthritis (CIA) rat model treated with methotrexate (MTX). Bioinformatic analysis revealed 485 differentially expressed proteins (DEPs) in CIA rats, among which 323 DEPs were restored to near-normal levels following MTX treatment. Overall, this strategy not only enhances the understanding of disease mechanisms and drug actions via serum proteomics but also offers a robust platform for identifying pharmacodynamic biomarkers relevant to disease prediction, diagnosis, and therapeutic evaluation.

Keywords: Pharmacodynamic biomarkers, Proteomic analysis, Mass spectrometry, Nanoparticles, Protein corona

How to Cite This Article: Tanaka H, Sato A, Yamamoto K. Proteomic Discovery of Pharmacodynamic Biomarkers Using a Highly Efficient Protein Corona-Based Strategy. Ann Pharm Pract Pharmacother. 2021;1:80-93. https://doi.org/10.51847/aeYhJe0KSD

Introduction

Serum contains a highly intricate mixture of proteins secreted by various tissues, along with a minor fraction derived from infectious agents or parasites within the body [1]. Notably, global alterations in serum protein composition—referred to as protein biomarkers—reflect changes induced by drug treatment, physiological states, or disease conditions [2]. Approximately 99% of the serum proteome is dominated by over 20 high-abundance proteins, such as albumin (50%–55%), immunoglobulins, transferrin, and apolipoproteins [3], while the remaining 1% comprises more than 10,000 low-abundance proteins (excluding post-translational modifications), typically present at μg/L or ng/L levels [4]. The wide dynamic range of serum proteins, spanning more than 10 orders of magnitude, along with complex post-translational modifications, renders serum one of the most challenging sub-proteomes to analyze [5]. Although strategies such as affinity-based depletion using antibodies or aptamers—limited to a few proteins like albumin and immunoglobulins [6, 7]—and labor-intensive offline fractionation at the protein or peptide level [8] have advanced, mass spectrometry (MS) and affinity proteomics remain the predominant approaches for serum protein discovery, accounting for nearly 90% of entries in the Plasma Proteome Database [9]. Currently, liquid chromatography-tandem mass spectrometry (LC-MS/MS) continues to be the standard method for serum proteomics. However, peptides derived from high-abundance proteins can suppress the detection of low-abundance proteins, which are often potential disease-relevant biomarkers [10]. Existing biomarker discovery approaches, relying on proteomics or DNA microarrays, primarily detect high-abundance proteins while low-abundance proteins remain largely hidden [11-14], limiting the identification of novel

pharmacodynamic biomarkers. Therefore, effective depletion of high-abundance proteins or enrichment of low-abundance proteins is critical to overcoming these limitations.

Protein corona (PC) forms when nanoparticles (NPs) rapidly adsorb surrounding proteins via hydrogen bonding, electrostatic interactions, van der Waals forces, and solvation effects [15-17]. PCs generally comprise high- and low-affinity proteins that constitute the hard and soft corona layers, respectively, with hydrophobic and electrostatic interactions primarily governing the formation of the hard and soft corona [18]. While high-abundance proteins are gradually replaced by low-abundance proteins, high-affinity proteins establish a relatively stable PC layer over time through the Vroman effect [19-21]. Recent MS-based proteomic studies demonstrated that PCs can capture low-abundance proteins from plasma [22-24], providing a promising approach for comprehensive serum proteome profiling, biomarker identification, and disease diagnostics. Iron oxide nanoparticles (IONPs) possess intrinsic magnetic properties and excellent biocompatibility and have been applied in diverse biomedical applications, including magnetic resonance imaging, treatment of iron-deficiency anemia, magnetic hyperthermia, and drug delivery [25]. Studies have shown that the PC of IONP-doped hydroxyapatite scaffolds can markedly enhance bone wound healing, highlighting their considerable biomedical potential [26]. Interestingly, variations in surface charge of IONP coatings have minimal impact on PC composition [27], and neutral or negatively charged IONPs exhibit longer circulation half-lives than positively charged ones [28]. Additionally, magnetic separation reduces protein aggregation and loss during PC washing compared to centrifugation [24, 29].

In this study, we synthesized and characterized silica-coated IONPs (Si-IONPs) to simultaneously deplete high-abundance proteins and enrich low-abundance proteins from serum using label-free quantitative proteomics **(Figure 1)**. We optimized the protein-to-Si-IONP ratio to evaluate enrichment efficiency and reproducibility. Using this PC-based strategy, we identified over 1,000 proteins across a wide dynamic range, approximately double the number detected in directly digested serum, with improved median coefficient of variation (CV) values, demonstrating superior reproducibility and efficiency in uncovering pharmacodynamic biomarkers. Applying this method to collagen-induced arthritis (CIA) rats treated with methotrexate (MTX) revealed that MTX effectively alleviated CIA symptoms and restored the balance of differentially expressed proteins (DEPs) and associated biological processes (BPs). Overall, this PC-based proteomic platform provides a scalable strategy for serum protein enrichment, enabling more comprehensive profiling and facilitating the discovery of pharmacodynamic biomarkers and therapeutic targets.

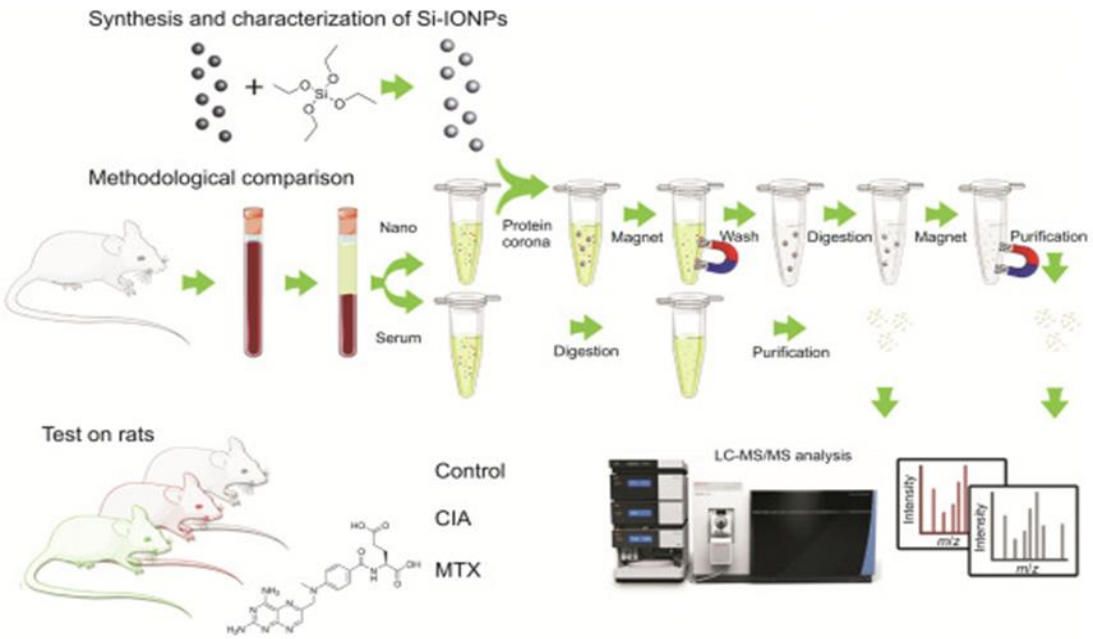

Figure 1. Illustration of the overall workflow depicting how silica-coated iron oxide nanoparticles (Si-IONPs) were employed to selectively remove high-abundance proteins and concentrate trace proteins. Abbreviations: CIA, collagen-induced arthritis; MTX, methotrexate; LC-MS/MS, liquid chromatography–tandem mass spectrometry; GO, Gene Ontology; BP, biological process.

Materials and Methods

All reagents used were of analytical grade unless otherwise noted. Ferric chloride hexahydrate ($FeCl_3·6H_2O$, 99%), calcium chloride dihydrate ($CaCl_2·2H_2O$), ammonium hydrogen carbonate (NH_4HCO_3), anhydrous sodium acetate (NaAc, 99%), sodium hydroxide (NaOH, 95%), potassium bromide (KBr, 99%), ethylene glycol (EG, 98%), absolute ethanol (EtOH, 99.5%), hexanediamine, and tetraethyl orthosilicate (TEOS, 98%) were supplied by Macklin Biochemical Co. (Shanghai, China). Gentamycin, L-glutamine, HEPES buffer, sodium bicarbonate ($NaHCO_3$), hypoxanthine, DL-dithiothreitol (DTT, 99%), iodoacetamide (IAA, 99%), MS-grade water and acetonitrile (ACN), as well as colorimetric peptide quantification and bicinchoninic acid (BCA) protein assay kits, were obtained from Thermo Fisher Scientific (Waltham, MA, USA). Formic acid (FA, 98%, MS grade) was obtained from TCI Europe NV (Zwijndrecht, Belgium). Sequencing-grade trypsin was purchased from Promega (Madison, WI, USA), and Oasis HLB cartridges were obtained from Waters Corporation (Milford, MA, USA). Urea (99.3%) was procured from Alfa Aesar (Heysham, UK). Trifluoroacetic acid (TFA, 99%), bovine type II collagen, incomplete Freund's adjuvant (IFA), and pentobarbital were purchased from Sigma-Aldrich (St. Louis, MO, USA). Methotrexate (MTX) was sourced from MedChemExpress (Monmouth Junction, NJ, USA). Multiplex Bio-Plex Pro cytokine assay kits (IL-6, IL-1β, IL-10, IL-17, TNF-α, GRO/KC) were supplied by Bio-Rad Laboratories (Hercules, CA, USA).

Synthesis and characterization of Si-IONPs

Synthesis

The magnetic nanoparticle cores were prepared through a solvothermal reaction following a previously described procedure [30, 31]. Briefly, 1 g of $FeCl_3·6H_2O$, 2 g of NaAc, and 6.5 mL of hexanediamine were dissolved in 30 mL of ethylene glycol while stirring continuously at 50 °C. The transparent reddish-brown solution was transferred into a Teflon-lined autoclave and maintained at 198 °C for six hours. After the reaction, the black precipitate was magnetically collected, washed several times with ultrapure water and ethanol, and lyophilized to obtain dry iron oxide nanoparticles (IONPs).

To apply a silica coating, 10 mg of the IONPs were redispersed in 50 mL of ethanol and sonicated until homogeneous. Subsequently, 0.5 mL of 4 M NaOH and 0.5 mL of TEOS were slowly introduced under mechanical agitation. The suspension was alternately stirred and sonicated for 2 h to ensure even coating formation. The silica-coated nanoparticles were rinsed repeatedly with ethanol and ultrapure water, then resuspended in 1 mL of ultrapure water to yield a 10 mg/mL stock dispersion.

Characterization

Multiple analytical platforms were employed to examine the physical and chemical attributes of Si-IONPs, including morphology, particle size, crystalline structure, surface chemistry, and magnetic response.

Transmission electron microscopy (TEM) was carried out using a JEOL JEM-200CX instrument (Tokyo, Japan). Samples were prepared by diluting the nanoparticle suspension with ultrapure water, sonicating for 5 min, and depositing 10 μL of a 50 mg/L dispersion onto a TEM grid. The grid was air-dried overnight, and 200 randomly selected particles were measured using Digital Micrograph 3.7 software to calculate the mean particle diameter.

The surface morphology was further visualized using a Hitachi S-4800 scanning electron microscope (SEM; Tokyo, Japan). A 20 μL aliquot of a 500 mg/L Si-IONP dispersion was sonicated briefly, dropped onto a monocrystalline silicon wafer, and dried overnight before imaging.

Hydrodynamic size and zeta potential were obtained with a Malvern Zetasizer Nano ZS90 (Malvern, UK). For both analyses, samples were diluted to 20 mg/L in ultrapure water. DLS readings were recorded at 25 °C with a 1-min averaging period, while surface charge was evaluated under identical conditions using the Smoluchowski model after a 2-min equilibration.

X-ray diffraction (XRD) was performed on a Bruker D8 Advance diffractometer (Karlsruhe, Germany). The dried nanoparticle powder was loaded into the XRD sample holder, flattened with a glass slide, and scanned. Diffraction peaks were matched with standard data from the PDF database using MDI Jade software.

Fourier transform infrared spectroscopy (FTIR) analysis was conducted using a Bruker Tensor 27 spectrometer (Karlsruhe, Germany). Finely ground nanoparticle powder was mixed with KBr, compressed into pellets at 27 MPa for 2 min, and scanned after background correction and water/carbon dioxide compensation to identify characteristic functional groups.

Magnetic properties were determined using a Lake Shore 7410 vibrating sample magnetometer (VSM; Columbus, OH, USA). Dried powder was packed into a sealed plastic tube (7 mm × 2 mm) and compacted prior to analysis. Saturation magnetization, coercivity, and remanence were then quantified.

Animal experiments

All animal procedures were conducted in accordance with the ethical standards approved by the China Animal Care and Use Committee and the Laboratory Animal Center of the China Academy of Chinese Medical Sciences. Twenty-one male Sprague–Dawley rats (Vital River Laboratory Animal Technology, Beijing, China), each weighing approximately 150 ± 10 g, were housed under controlled environmental conditions—12-hour light/dark cycle, 22 ± 2 °C temperature, and 55 ± 5% humidity—and provided unrestricted access to food and water for one week to acclimate. After adaptation, the animals were separated into two groups: the control group (n = 5) and the collagen-induced arthritis (CIA) model group (n = 16). The CIA model was established by intradermally administering a homogeneous emulsion composed of bovine type II collagen and incomplete Freund's adjuvant (IFA) at the base of the tail on days 0 and 7. The control rats were injected with the same volume of normal saline. On day 14, the rats showing arthritis scores greater than four were randomly selected (n = 10) and subdivided into untreated CIA (n = 5) and methotrexate-treated (MTX) (n = 5) groups. Rats in the MTX group received intraperitoneal injections of MTX (0.5 mg/kg) twice weekly for four consecutive weeks, while the control and CIA groups were given normal saline on the same schedule. Body weight was recorded twice per week, and arthritic progression was evaluated weekly using a 0–5 scoring system: 0, no inflammation; 1, slight redness or swelling in the ankle; 2, moderate swelling extending to the midfoot; 3, inflammation affecting the foot except toes; 4, swelling of the whole foot; and 5, severe inflammation with limited mobility. After 42 days (post-final MTX administration), blood samples were collected under anesthesia, left to clot for 4 h at room temperature, and centrifuged at 4,000 r/min for 10 min to isolate serum, which was then stored at −80 °C for later use.

Luminex multiplex assay for cytokine analysis

To measure serum cytokine concentrations (IL-6, IL-1β, IL-10, IL-17, TNF-α, and GRO/KC), a Luminex multiplex immunoassay was performed. All reagents and samples were equilibrated to room temperature before analysis, and sera were diluted 1:4 (v/v) using phosphate-buffered saline (PBS). The assays were conducted strictly following the manufacturer's instructions, and each measurement was performed in triplicate to ensure precision.

Micro-computed tomography (micro-CT) imaging

Three-dimensional (3D) imaging of the rats' ankle joints was performed using a Bruker SkyScan 1174 micro-CT scanner (Karlsruhe, Germany). Joints from the control, CIA, and MTX groups were scanned with the following parameters: 50 kV X-ray voltage, 800 μA current, image resolution of 1304 × 1024, and a region of interest covering 1,000 slices (approximately 14.5 mm) starting from the calcaneus. Image reconstruction was performed using N-Recon software, and bone structural parameters, including volume and surface area, were determined using CT-Analyzer software (Bruker, Karlsruhe, Germany).

Protein corona (PC) preparation and proteomic workflow

For the formation of the protein corona, serum samples from control rats were thawed at 4 °C, pooled (10 μL each), and diluted 1:100 with 0.01 M PBS. The silica-coated iron oxide nanoparticles (Si-IONPs) were prepared at 20 mg/mL and sonicated for 10 minutes to ensure uniform dispersion. To establish the optimal serum-to-nanoparticle ratio, 10 μL of Si-IONP suspensions with different concentrations (0.5–20 mg/mL) were added to 200 μL of 1% serum and incubated at 28 °C for 1 hour under shaking (600 r/min). After magnetic separation using a DynaMag™-2 Magnet (Thermo Fisher Scientific, USA) for 6 seconds, protein levels in the supernatant were determined with a BCA protein assay kit, using 1% serum as the reference concentration.

For proteomic analysis, 10 μL of Si-IONPs (10 mg/mL) were combined with 200 μL of diluted serum and incubated at 28 °C for 1 hour (600 r/min). After separation by magnet, the nanoparticles were washed three times with 200 μL PBS to remove unbound proteins. The adsorbed proteins were reduced with three μL of 200 mM DTT at 55 °C for 45 minutes, followed by alkylation with four μL of 400 mM IAA for 30 minutes at room temperature in the dark. Protein digestion was then carried out by adding four μL of 0.5 μg/μL trypsin, 30 μL of 2 M urea in PBS, and 30 μL of 1 mM $CaCl_2$ in 50 mM NH_4HCO_3, and incubating for 12 hours at 28 °C (300

r/min). The reaction was quenched with 200 μL of 0.1% TFA, and the nanoparticles were magnetically separated. The collected supernatant and two washes with 0.1% TFA were pooled, desalted using an Oasis HLB extraction cartridge, and eluted with 0.1% TFA in 70% acetonitrile.

In the control serum digestion (serum group), 10 μL of PBS replaced the Si-IONPs, and identical digestion and processing steps were applied without magnetic isolation. The peptide yield was quantified with a colorimetric peptide assay kit (Thermo Fisher Scientific, USA).

This optimized PC-based proteomic approach was subsequently applied to identify key serum biomarkers associated with CIA pathology and methotrexate-mediated therapeutic effects. Serum from control, CIA, and MTX rats (n = 3 per group) was processed under identical conditions to the nano group for comparative proteomic profiling.

Data-dependent acquisition (DDA)

Peptide samples were vacuum-dried and reconstituted in a solvent containing 0.1% formic acid (FA) and 1% acetonitrile (ACN) to reach a final concentration between 0.5 and 1 μg/μL. The reconstituted peptides were analyzed using a nano-liquid chromatography-tandem mass spectrometry (nano-LC-MS/MS) system equipped with an Ultimate 3000 RSLC nano system coupled to an Orbitrap Fusion Lumos Tribrid Mass Spectrometer (Thermo Fisher Scientific, USA). The mobile phase A consisted of LC/MS-grade water with 0.1% FA, while mobile phase B comprised 80% ACN with 0.1% FA. A 1 μL aliquot of peptide sample was loaded onto a trapping column (Thermo Fisher Scientific, part no. 164535) and subsequently separated on an analytical column (part no. 164941) at a constant flow rate of 300 nL/min. The gradient profile was set as follows: 6%–40% B over 79 minutes, followed by 40%–90% B for 1 minute, maintained at 90% B until 85 minutes, and then re-equilibrated to 6% B at 85.1 minutes, with a total run time of 95 minutes. The peptides were ionized using a nano-electrospray ionization source and introduced into the Orbitrap mass spectrometer operating in DDA mode. Full MS1 scans were acquired at a resolution of 120,000 (FWHM) within the m/z range of 350–1550. The 25 most abundant precursor ions from each MS1 scan were subjected to MS/MS fragmentation via higher-energy collisional dissociation (HCD) at 30% energy, and the resulting MS/MS spectra were recorded in the ion trap within an m/z range of 200–1400.

Statistical analysis

All experiments were independently repeated at least three times, and the data were expressed as mean ± standard deviation (SD). Statistical comparisons were performed using one-way analysis of variance (ANOVA) followed by the least significant difference (LSD) post hoc test in SPSS Statistics 19.0 software, with a significance level set at $P < 0.05$.

Characterization of Si-IONPs

A straightforward synthesis route was employed to produce silica-coated iron oxide nanoparticles (Si-IONPs) with excellent magnetic responsiveness and colloidal stability, suitable for protein adsorption and LC-MS/MS proteomic applications. Transmission electron microscopy (TEM) and scanning electron microscopy (SEM) analyses confirmed that the nanoparticles were well-dispersed and nearly spherical, with an average size of 93 ± 10 nm **(Figures 2a and 2b)**. Dynamic light scattering (DLS) measurements **(Figure 2c)** revealed a hydrodynamic diameter of approximately 190 nm, a polydispersity index of 0.125, and a surface zeta potential of −2.6 mV, reflecting good dispersibility in aqueous solution. The X-ray diffraction (XRD) pattern **(Figure 2d)** exhibited diffraction peaks corresponding to the spinel Fe_3O_4 phase (PDF 65-3107), without any additional impurity peaks, confirming high crystallinity of the magnetic core. In the Fourier-transform infrared (FTIR) spectrum **(Figure 2e)**, the absorption band at 570 cm^{-1} was attributed to Fe–O vibrations of Fe_3O_4 [32], while the band at 1630 cm^{-1} indicated $–NH_2$ groups [33] beneficial for further chemical modification. The Si–O stretching peak at 1086 cm^{-1} corresponded to the silica layer [34], and together with the XRD results, it suggested that the SiO_2 coating existed in an amorphous form [35]. Magnetization analysis **(Figure 2f)** demonstrated a saturation magnetization value of 87.96 emu/g with negligible coercivity and remanence, signifying strong superparamagnetic behavior [36]. Overall, these findings verify that the synthesized Si-IONPs possess excellent aqueous dispersibility and magnetic performance, making them highly suitable for biotechnological and biomedical proteomic enrichment applications.

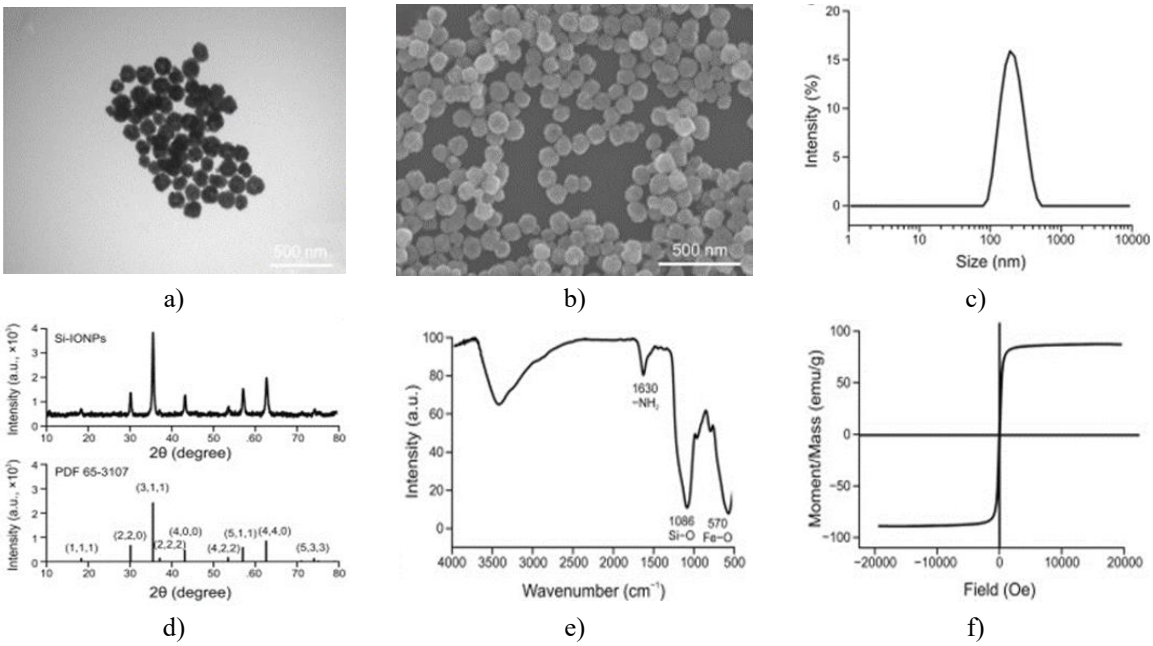

Figure 2. Characterization of silica-coated iron oxide nanoparticles (Si-IONPs). (a) Transmission electron microscopy (TEM) image showing the morphology of Si-IONPs. (b) Scanning electron microscopy (SEM) image depicting surface features of the synthesized nanoparticles. (c) Dynamic light scattering (DLS) profile indicating the particle size distribution. (d) X-ray diffraction (XRD) pattern confirming crystalline structure. (e) Fourier transform infrared (FTIR) spectrum illustrating the characteristic functional groups. (f) Vibrating sample magnetometer (VSM) curve showing magnetic properties. PDF: powder diffraction file.

PC-based proteomic analysis strategy

The amount of protein that adhered to the surface of Si-IONPs was determined by comparing the initial protein concentration with that remaining in the supernatant. Increasing Si-IONP concentrations led to greater protein adsorption until the curve plateaued at 10 mg/mL, indicating saturation. Therefore, this concentration was adopted for subsequent proteomic profiling of rat serum. For the nanoparticle-based (nano) group, 10 µL of Si-IONPs were incubated with three diluted serum samples at 28 °C for 1 hour to establish a stable protein corona (PC). The nanoparticle–protein complexes were magnetically separated from unbound proteins, followed by reduction, enzymatic digestion, and elution steps. Processing one batch of 16 PC samples required approximately 16 hours. The resulting peptides were subjected to LC–MS/MS analysis in data-dependent acquisition (DDA) mode using a 90-minute gradient. Peptide identification and quantification were carried out with Proteome Discoverer software. The control serum group was prepared by mixing diluted serum samples with 10 µL of 0.01 M PBS and processed identically to the nano group for digestion and analysis.

Using Si-IONPs markedly increased both the detection and quantification of serum proteins across all dilutions. The nano group yielded 1,070 identifiable proteins, compared to only 573 in the serum group. Among them, 507 proteins were shared, while 563 were unique to the nano group and 66 were exclusive to the serum group **(Figure 3a)**. Statistical evaluation revealed median coefficients of variation (CVs) of 12.56% and 11.03% for total proteins in the nano and serum groups, respectively, with an adjusted P value of 0.0043 **(Figure 3b, left)**. For the 507 overlapping proteins, the CVs were 8.42% (nano) and 10.49% (serum), with P (adj) = 0.0067 **(Figure 3b, right)**, signifying robust reproducibility of the Si-IONPs-based approach in detecting subtle abundance differences.

In the nano group, protein abundance was distributed as follows: 147 proteins at mg/L, 342 at µg/L, 175 at ng/L, and 406 unquantified. Of the 563 unique nano proteins, 14, 170, 136, and 243 fell within these respective categories. In contrast, the serum group contained 138, 202, 46, and 187 proteins in the same abundance brackets, with 5, 30, 7, and 24 among its 66 unique proteins **(Figure 3c)**. Mapping these proteins against the dynamic range of the serum proteome **(Figure 3d)** using data from The Human Protein Atlas (https://www.proteinatlas.org/humanproteome/blood) revealed that Si-IONPs enabled identification across nearly the entire dynamic range.

A total of 1,136 proteins from both groups were compared against a complete serum protein reference database, confirming that Si-IONPs effectively depleted abundant proteins while enriching low-abundance ones. Specifically, 108 proteins showed significant depletion, and 473 were enriched following nanoparticle treatment. Notably, highly abundant serum proteins—such as complement C3, alpha-2-macroglobulin, alpha-1-acid glycoprotein, ceruloplasmin, peptidoglycan recognition protein 2, angiotensinogen, and albumin—were reduced by more than 80 percent.

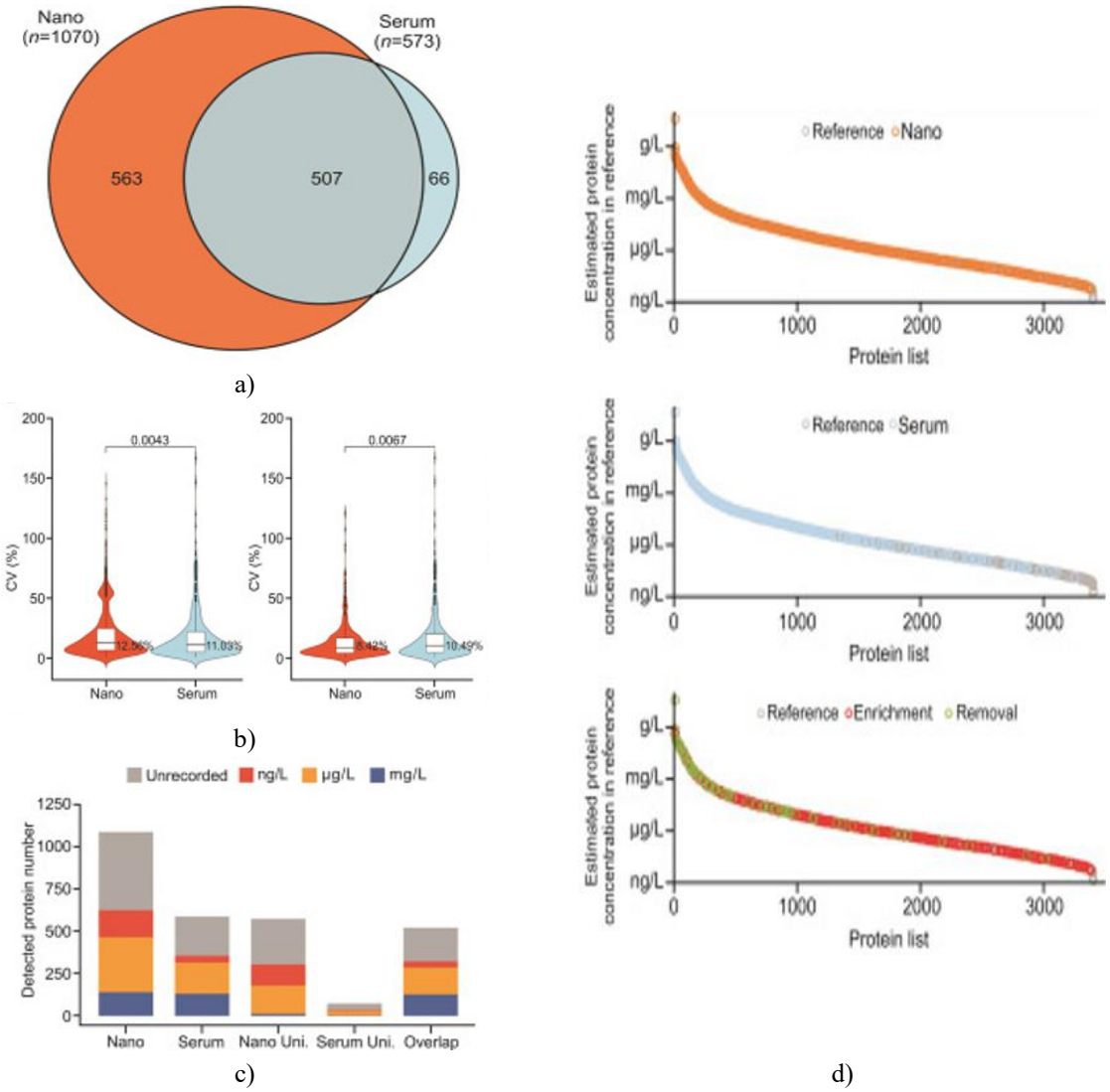

Figure 3. Proteomic outcomes derived from the protein corona (PC)-based analytical approach. (a) Venn diagram displaying the distribution of proteins detected in both nano-treated and untreated serum groups. (b) Variation coefficients of total proteins (left) and shared proteins (right) illustrate the reproducibility of the silica-coated iron oxide nanoparticles (Si-IONPs). (c) Comparison of protein counts categorized by concentration range across the nano and serum samples (unrecorded refers to proteins without concentration data in the reference database). “Nano Uni.” and “Serum Uni.” indicate proteins found exclusively in either the nano or serum group, while “Overlap” refers to proteins detected in both. (d) Relative protein intensity distribution in nano and serum samples compared with the human serum protein MS intensity database (reference = baseline proteins; nano = nanoparticle-bound proteins; serum = native serum proteins; enrichment = proteins concentrated by Si-IONPs; removal = proteins depleted by Si-IONPs). CV: coefficient of variation.

To highlight the distinctive analytical benefits provided by Si-IONPs, all related genes were subjected to Gene Ontology (GO) enrichment analysis using R packages. As illustrated in **Figure 4a**, 4,440 biological processes (BPs)—equivalent to 83.8% of all enriched processes—were shared between the nano and serum datasets, while

801 (15.1%) and 58 (1.1%) were uniquely observed in the nano and serum groups, respectively. Further comparison of the overlapping BPs revealed that Si-IONP treatment markedly increased the number of proteins associated with each BP (D-value > 0) **(Figure 4b)**. Analysis of the adjusted P-values [P(adj)] demonstrated median values of 0.244 for the nano group and 0.317 for the serum group, with 1,339 BPs in the nano group exhibiting P(adj) < 0.05—380 more than in the serum dataset **(Figure 4c)**. These observations confirm that the Si-IONP-assisted workflow enhances both the depth and statistical reliability of GO enrichment results, offering a stronger basis for identifying potential pharmacodynamic biomarkers.

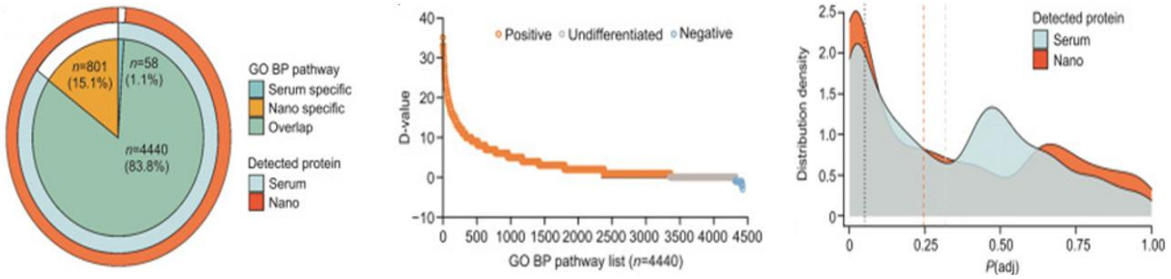

a) b) c)

Figure 4. Gene Ontology (GO) enrichment analysis using the protein corona (PC)-based proteomic approach. (a) Pie chart illustrating the distribution of enriched GO biological processes (BPs) and corresponding proteins in the nano-treated and serum groups. "Serum-specific" and "Nano-specific" indicate the unique BPs identified in each group, while "Overlap" denotes shared BPs between them. (b) The difference in protein counts (D-value = $n_{Nano} - n_{Serum}$) across 4,440 overlapping GO BP pathways, where n_Nano and n_Serum represent the number of proteins per pathway in the nano and serum groups, respectively. (c) Distribution of adjusted P-values [P(adj)] for the overlapping BPs in GO enrichment analysis.

The identification of novel protein biomarkers that define disease states or predict disease development is a critical step in early diagnosis and therapeutic planning. However, the inherent complexity of serum proteins continues to hinder biomarker discovery. Since its introduction, research on the formation of protein coronas (PCs) has advanced the understanding of the serum proteome, as proteins interact with nanoparticles through specific or nonspecific adsorption processes [37]. The composition of PCs is largely determined by both the physicochemical traits of nanoparticles and the surrounding protein milieu [38]. Moreover, biological processes such as pharmacokinetics, cellular internalization, and toxicity can significantly influence PC formation [39, 40]. Hence, a deeper insight into PC dynamics not only assists in the rational design of nanomedicines for targeted therapy, imaging, and diagnostics but also provides valuable information on alterations within biological fluids like serum and blood.

Currently, two primary proteomic strategies—targeted and untargeted—are used to investigate serum proteins [41, 42]. Each method presents distinct advantages and limitations. Targeted proteomics offers high sensitivity and absolute quantification, making it particularly effective for validating biomarkers across experimental conditions, while untargeted proteomics is more suitable for discovering new biomarkers during preliminary research phases [43].

Recent developments in PC-based proteomics using untargeted analysis have focused on improving the detection of low-abundance proteins by reducing the interference of dominant serum proteins. For example, Tiambeng *et al*. [44] developed superparamagnetic iron oxide nanoparticles (IONPs) functionalized with N-(3-(triethoxysilyl)propyl)buta-2,3-dienamide and a cardiac troponin I (cTnI)-binding peptide, enabling efficient enrichment of cTnI and depletion of albumin. Similarly, Blume *et al*. [24] screened 43 IONP formulations with distinct physicochemical traits and optimized a set of 10 nanoparticles for unbiased human serum protein profiling, which later became the foundation for Seer Inc.'s Proteograph Assay Kit [45]. Using this optimized approach, they detected 1,184 protein groups, with 761 displaying coefficient of variation (CV) values below 20%—a benchmark for in-vitro diagnostic reproducibility.

In comparison, our synthesized Si-IONPs achieved similar analytical power through a simpler synthesis process and minimal surface modification. These nanoparticles successfully removed at least 15 high-abundance serum proteins while identifying 1,070 distinct protein groups, of which 742 exhibited CV < 20%. These findings are

consistent with the performance of the Seer kit and the optimized IONP panels reported by Blume *et al*. [24, 45], underscoring the robustness and efficiency of Si-IONPs for serum proteomics.

Earlier studies have shown that albumin and fibrinogen exhibit strong binding affinities to nanoparticles, often dominating the adsorbed protein layer [46]. Interestingly, our Si-IONPs demonstrated the ability to simultaneously enrich low-abundance proteins while effectively depleting highly abundant ones, suggesting their utility for broad-spectrum proteomic profiling. Given their wide protein coverage, these Si-IONPs present significant potential for large-scale pharmacodynamic biomarker discovery. Moreover, evidence indicates that employing peptide pre-fractionation—such as separating digested peptides into multiple fractions using reversed-phase high-performance liquid chromatography (HPLC)—can markedly increase the number of detectable proteins [8]. We plan to integrate this pre-fractionation strategy in future work to further enhance serum proteome coverage.

In conclusion, the application of Si-IONPs yielded an efficient, reproducible, and unbiased enrichment of low-abundance serum proteins, substantially increasing the number of identified proteins compared with the untreated serum group. Subsequently, this method was applied to serum samples from collagen-induced arthritis (CIA) rats to further evaluate the capability of Si-IONPs in identifying pharmacodynamic biomarkers and potential therapeutic targets.

Application: identification of CIA biomarkers and MTX therapeutic targets

To assess the pharmacological efficacy of methotrexate (MTX) in collagen-induced arthritis (CIA), a rat CIA model was effectively generated. Several parameters, including body weight, arthritis severity scores, micro-computed tomography (micro-CT) findings, and serum levels of inflammatory cytokines, were used to evaluate disease progression and therapeutic response [47, 48]. Relative to the healthy control rats, the CIA group exhibited a progressive decline in body weight accompanied by a notable rise in arthritis scores. Treatment with MTX significantly mitigated these effects, leading to weight recovery and reduced arthritis scores when compared with the untreated CIA rats **(Figure 5a)**. Moreover, visual inspection revealed substantial paw swelling in the CIA group, which was remarkably alleviated following MTX administration **(Figure 5b, upper panel**).

Micro-CT imaging of the ankle joints further demonstrated extensive joint damage in CIA rats, characterized by surface roughness, joint space narrowing, and bone fusion, whereas MTX-treated animals displayed pronounced recovery with reduced bone erosion after 28 days of therapy **(Figure 5b, lower panel)**.

In addition, the serum concentrations of key inflammatory mediators, including IL-1β, IL-6, IL-17, IL-10, TNF-α, and GRO/KC, were quantified. The CIA group showed significantly elevated levels of IL-1β, IL-6, IL-17, TNF-α, and GRO/KC, accompanied by a marked suppression of the anti-inflammatory cytokine IL-10 compared to controls. After 28 days of MTX administration, these cytokine imbalances were notably corrected, trending toward normal physiological levels **(Figure 5c)**. Collectively, these findings confirm that the CIA model was successfully established and that MTX effectively ameliorated the pathological manifestations of arthritis in treated rats.

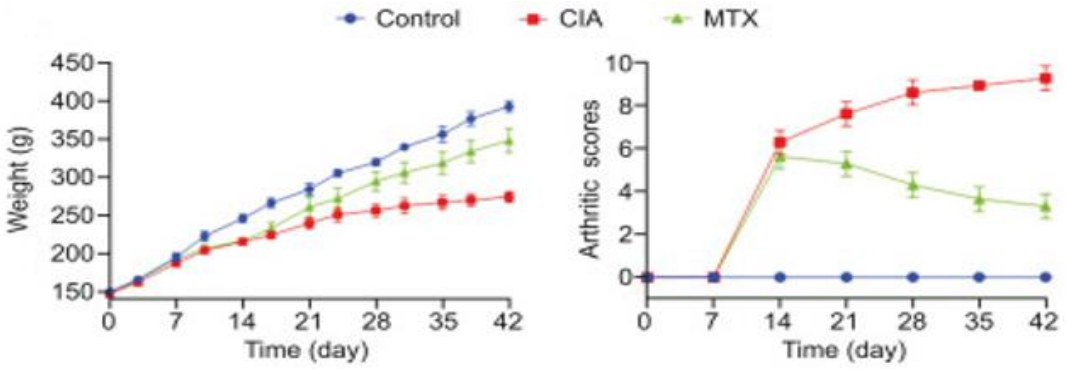

a)

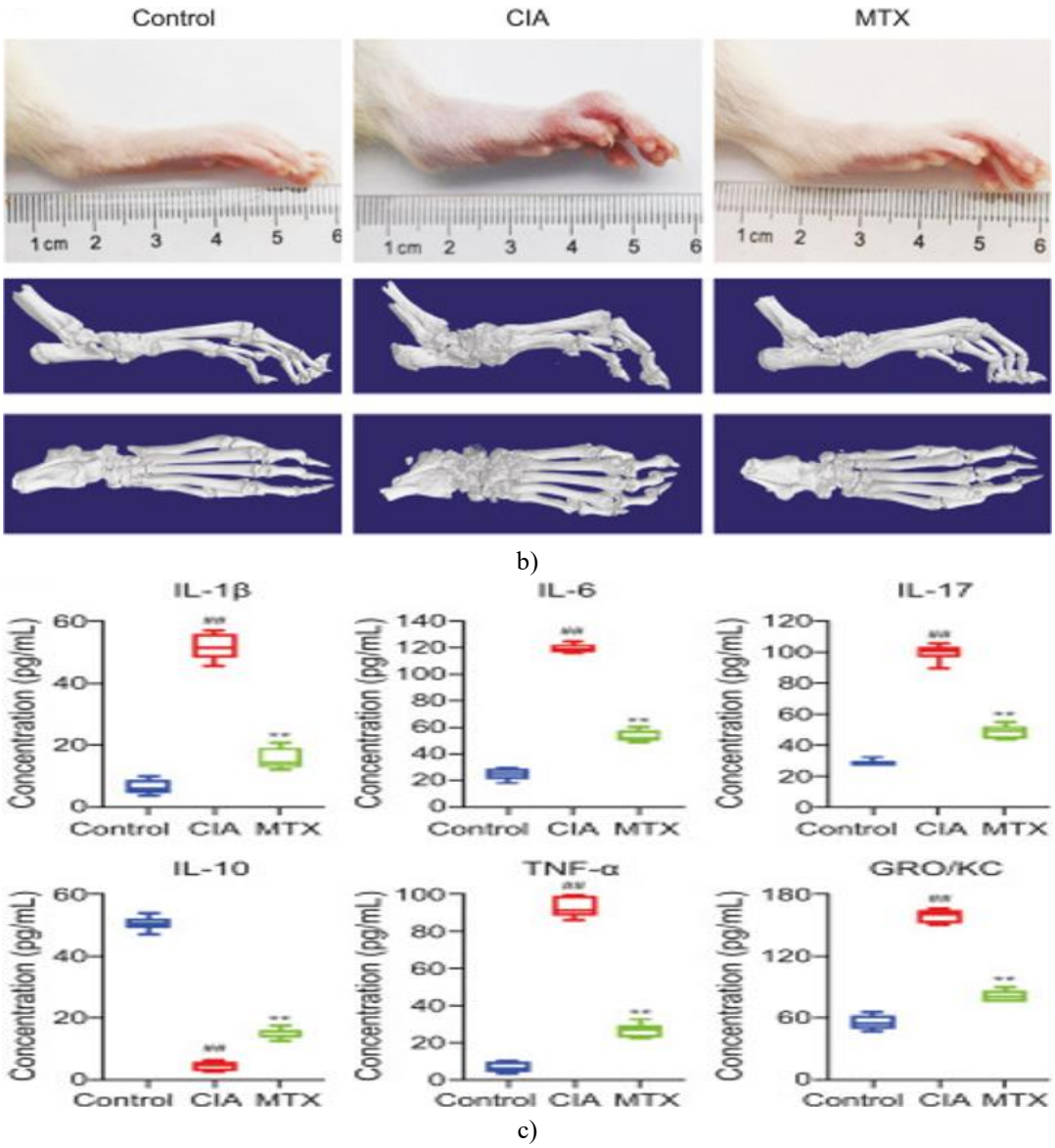

Figure 5. Anti-arthritic efficacy of methotrexate (MTX) in collagen-induced arthritis (CIA) rats. (a) MTX administration influenced both body weight (left) and arthritis severity scores (right) across experimental groups. (b) Representative images of rat paws (top) and micro-computed tomography (micro-CT) scans (bottom) reveal the morphological and structural differences among control, CIA, and MTX-treated groups. (c) Serum cytokine analysis shows the effects of MTX on interleukin-1β (IL-1β), IL-6, IL-17, IL-10, tumor necrosis factor-α (TNF-α), and growth-regulated oncogene/keratinocyte chemoattractant (GRO/KC). # $P < 0.01$, CIA vs. control; * $P < 0.01$, MTX vs. CIA.

To investigate serum proteomic alterations caused by CIA and elucidate the molecular mechanism behind MTX's therapeutic action, serum proteins from each group were enriched using silica-coated iron oxide nanoparticles (Si-IONPs). Through protein corona (PC)-based proteomic analysis, 986, 1,078, and 965 proteins were identified in the control, CIA, and MTX groups, respectively (n = 3). A heat map **Figure 6a** illustrated substantial increases in protein abundance in the CIA group compared to controls, whereas MTX treatment normalized these aberrant expression patterns. Notably, the proteomic profile of MTX-treated rats closely resembled that of healthy controls, indicating that MTX effectively mitigates CIA-induced protein dysregulation. Differentially expressed proteins (DEPs) were determined using the criteria P(adj) < 0.05 and fold change > 1.2. As displayed in **Figures 6b and 6c**, the CIA/control comparison revealed 485 DEPs (399 upregulated and 86 downregulated), while the CIA/MTX comparison showed 519 DEPs (409 upregulated and 110 downregulated). These findings highlight the utility of PC-based proteomics for uncovering pharmacodynamic biomarkers and potential therapeutic targets.

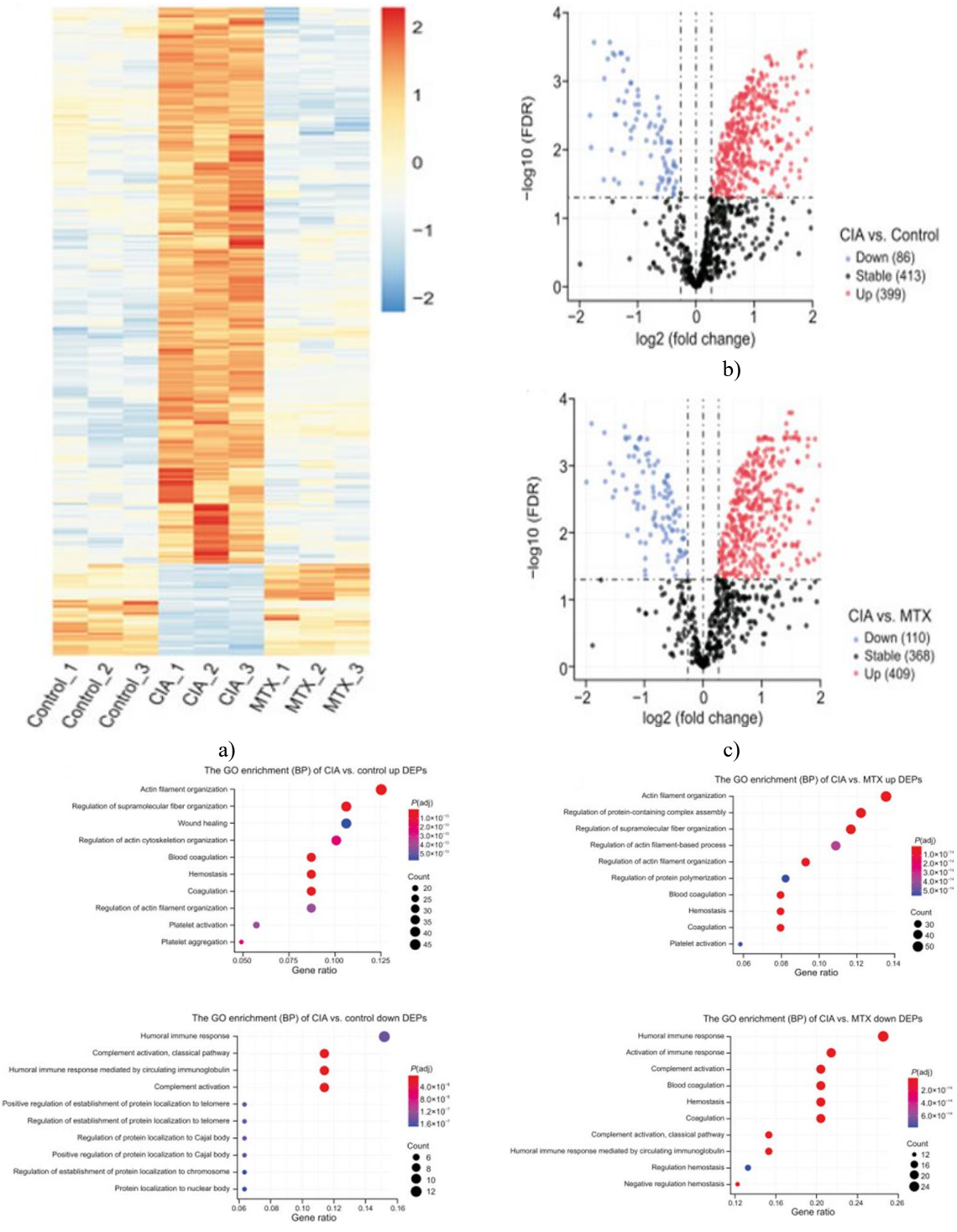

Figure 6. Analysis of differentially expressed proteins (DEPs) and associated biological processes (BPs) identified from the comparisons between collagen-induced arthritis (CIA) versus control and CIA versus methotrexate (MTX) groups. (a) The heat map displays gene expression profiles among control, CIA, and MTX groups, where red represents upregulated and blue represents downregulated proteins. (b) and (c) show volcano plots of DEPs for the CIA/control and CIA/MTX comparisons, respectively. (d) Gene Ontology (GO) enrichment analysis of the CIA/control comparison reveals the top 10 upregulated (upper) and downregulated (lower) BP categories, while (e) presents the corresponding GO terms for the CIA/MTX comparison. FDR indicates the false discovery rate.

To gain deeper insight into the mechanisms underlying CIA pathogenesis and MTX's therapeutic impact, GO enrichment analysis was performed on the DEPs from both CIA/control and CIA/MTX groups. In the CIA/control

comparison, upregulated proteins were predominantly involved in actin filament organization, regulation of supramolecular fiber organization, and wound healing **(Figure 6d, top)**. Conversely, the downregulated DEPs were enriched in pathways related to the humoral immune response, complement activation via the classical pathway, and antibody-mediated immune responses **(Figure 6d, bottom)**. In the CIA/MTX comparison, upregulated proteins were again mainly associated with cytoskeletal and structural regulation processes such as actin filament organization and supramolecular complex assembly **(Figure 6e, top)**. Meanwhile, the downregulated proteins were significantly linked to immune system processes, including humoral immune response, activation of immune response, and complement activation **(Figure 6e, bottom)**.

Further comparative analysis revealed that MTX effectively reversed many CIA-induced disruptions in biological processes. Among the elevated BPs, processes like actin filament organization, regulation of supramolecular fiber organization, blood coagulation, hemostasis, and platelet activation were notably normalized following MTX treatment. Similarly, MTX restored the suppression of humoral immune response, complement activation (including the classical pathway), and antibody-mediated immune functions observed in CIA rats. As this study primarily aimed to expand the serum proteome coverage and identify relevant biological processes, no additional experimental validation was conducted at this stage. The identified DEPs and enriched BPs will be the focus of future studies to confirm potential MTX targets within the CIA model.

This study successfully demonstrated the application of the PC-based proteomic analysis approach in a CIA rat model, using MTX as a reference therapeutic agent. Both pharmacological and proteomic analyses confirmed MTX's pronounced anti-arthritic effects. Among the 485 DEPs identified in the CIA model, 323 were restored toward normal expression following MTX treatment. Whether these DEPs can serve as pharmacodynamic biomarkers of CIA or direct molecular targets of MTX requires further investigation

Conclusion

In summary, a straightforward synthesis of silica-coated iron oxide nanoparticles (Si-IONPs) was achieved, enabling the development of a PC-based proteomic analysis strategy that broadened the scope of serum proteomics. This method efficiently reduced high-abundance proteins while enhancing the detection of low-abundance serum proteins with strong reproducibility. Although further mechanistic studies are warranted, this strategy holds great promise for deepening our understanding of disease mechanisms and drug actions through serum proteomics. Moreover, it opens new avenues for identifying pharmacodynamic biomarkers relevant to disease prediction, diagnosis, and treatment. Future applications could extend to other biological fluids for detecting diverse biomolecules—such as nucleic acids, sugars, and metabolites—pending experimental validation.

Acknowledgments: None

Conflict of Interest: None

Financial Support: None

Ethics Statement: None

References

1. Lamb JR, Jennings LL, Gudmundsdottir V, Gudnason V, Emilsson V. It's in Our Blood: A Glimpse of Personalized Medicine. Trends Mol Med. 2021;27(1):20-30.
2. Anderson NL. The clinical plasma proteome: a survey of clinical assays for proteins in plasma and serum. Clin Chem. 2010;56(2):177-85.
3. Zhang H, Yi EC, Li XJ, Mallick P, Kelly-Spratt KS, Masselon CD, et al. High throughput quantitative analysis of serum proteins using glycopeptide capture and liquid chromatography mass spectrometry. Mol Cell Proteomics. 2005;4(2):144-55.
4. Tirumalai RS, Chan KC, Prieto DA, Issaq HJ, Conrads TP, Veenstra TD. Characterization of the low molecular weight human serum proteome. Mol Cell Proteomics. 2003;2(10):1096-103.

5. Kim MS, Pinto SM, Getnet D, Nirujogi RS, Manda SS, Chaerkady R, et al. A draft map of the human proteome. Nature. 2014;509(7502):575-81.
6. Dalle Carbonare L, Manfredi M, Caviglia G, Conte E, Robotti E, Marengo E, et al. Can half-marathon affect overall health? The yin-yang of sport. J Proteomics. 2018;170:80-7.
7. Urbas L, Brne P, Gabor B, Barut M, Strlic M, Petric TC, et al. Depletion of high-abundance proteins from human plasma using a combination of an affinity and pseudo-affinity column. J Chromatogr A. 2009;1216(13):2689-94.
8. Wang H, Dey KK, Chen PC, Li Y, Niu M, Cho JH, et al. Integrated analysis of ultra-deep proteomes in cortex, cerebrospinal fluid and serum reveals a mitochondrial signature in Alzheimer's disease. Mol Neurodegener. 2020;15(1):43.
9. Suhre K, McCarthy MI, Schwenk JM. Genetics meets proteomics: perspectives for large population-based studies. Nat Rev Genet. 2021;22(1):19-37.
10. Hortin GL, Sviridov D, Anderson NL. High-abundance polypeptides of the human plasma proteome comprising the top 4 logs of polypeptide abundance. Clin Chem. 2008;54(10):1608-16.
11. Kulasingam V, Diamandis EP. Strategies for discovering novel cancer biomarkers through utilization of emerging technologies. Nat Clin Pract Oncol. 2008;5(10):588-99.
12. Lee PY, Osman J, Low TY, Jamal R. Plasma/serum proteomics: depletion strategies for reducing high-abundance proteins for biomarker discovery. Bioanalysis. 2019;11(19):1799-812.
13. Kumar V, Ray S, Ghantasala S, Srivastava S. An Integrated Quantitative Proteomics Workflow for Cancer Biomarker Discovery and Validation in Plasma. Front Oncol. 2020;10:543997.
14. Li Y, Yuan H, Dai Z, Zhang W, Zhang X, Zhao B, et al. Integrated proteomic sample preparation with combination of on-line high-abundance protein depletion, denaturation, reduction, desalting and digestion to achieve high throughput plasma proteome quantification. Anal Chim Acta. 2021;1154:338343.
15. Saptarshi SR, Duschl A, Lopata AL. Interaction of nanoparticles with proteins: relation to bio-reactivity of the nanoparticle. J Nanobiotechnology. 2013;11:26.
16. Wan S, Kelly PM, Mahon E, Stöckmann H, Rudd PM, Caruso F, et al. The "sweet" side of the protein corona: effects of glycosylation on nanoparticle-cell interactions. ACS Nano. 2015;9(2):2157-66.
17. Monopoli MP, Aberg C, Salvati A, Dawson KA. Biomolecular coronas provide the biological identity of nanosized materials. Nat Nanotechnol. 2012;7(12):779-86.
18. Pinals RL, Yang D, Rosenberg DJ, Chaudhary T, Crothers AR, Iavarone AT, et al. Quantitative Protein Corona Composition and Dynamics on Carbon Nanotubes in Biological Environments. Angew Chem Int Ed Engl. 2020;59(52):23668-77.
19. Elechalawar CK, Hossen MN, McNally L, Bhattacharya R, Mukherjee P. Analysing the nanoparticle-protein corona for potential molecular target identification. J Control Release. 2020;322:122-36.
20. VROMAN L. Effect of absorbed proteins on the wettability of hydrophilic and hydrophobic solids. Nature. 1962;196:476-7.
21. Giri K, Shameer K, Zimmermann MT, Saha S, Chakraborty PK, Sharma A, et al. Understanding protein-nanoparticle interaction: a new gateway to disease therapeutics. Bioconjug Chem. 2014;25(6):1078-90.
22. Liu Y, Wang J, Xiong Q, Hornburg D, Tao W, Farokhzad OC. Nano-Bio Interactions in Cancer: From Therapeutics Delivery to Early Detection. Acc Chem Res. 2021;54(2):291-301.
23. Hadjidemetriou M, McAdam S, Garner G, Thackeray C, Knight D, Smith D, et al. The Human In Vivo Biomolecule Corona onto PEGylated Liposomes: A Proof-of-Concept Clinical Study. Adv Mater. 2019;31(4):e1803335.
24. Blume JE, Manning WC, Troiano G, Hornburg D, Figa M, Hesterberg L, et al. Rapid, deep and precise profiling of the plasma proteome with multi-nanoparticle protein corona. Nat Commun. 2020;11(1):3662.
25. Cardoso VF, Francesko A, Ribeiro C, Bañobre-López M, Martins P, Lanceros-Mendez S. Advances in Magnetic Nanoparticles for Biomedical Applications. Adv Healthc Mater. 2018;7(5).
26. Zhu Y, Jiang P, Luo B, Lan F, He J, Wu Y. Dynamic protein corona influences immune-modulating osteogenesis in magnetic nanoparticle (MNP)-infiltrated bone regeneration scaffolds in vivo. Nanoscale. 2019;11(14):6817-27.
27. Portilla Y, Mellid S, Paradela A, Ramos-Fernández A, Daviu N, Sanz-Ortega L, et al. Iron Oxide Nanoparticle Coatings Dictate Cell Outcomes Despite the Influence of Protein Coronas. ACS Appl Mater Interfaces. 2021;13(7):7924-44.

28. Sakulkhu U, Mahmoudi M, Maurizi L, Salaklang J, Hofmann H. Protein corona composition of superparamagnetic iron oxide nanoparticles with various physico-chemical properties and coatings. Sci Rep. 2014;4:5020.
29. Bonvin D, Chiappe D, Moniatte M, Hofmann H, Mionić Ebersold M. Methods of protein corona isolation for magnetic nanoparticles. Analyst. 2017;142(20):3805-15.
30. Wang L, Bao J, Wang L, Zhang F, Li Y. One-pot synthesis and bioapplication of amine-functionalized magnetite nanoparticles and hollow nanospheres. Chemistry. 2006;12(24):6341-7.
31. Yin ZZ, Li Y, Jiang LP, Rana RK, Zhu JJ. Synthesis and electrocatalytic activity of haemin-functionalised iron(II, III) oxide nanoparticles. Anal Chim Acta. 2013;781:48-53.
32. Ozkaya T, Toprak MS, Baykal A, Kavas H, Köseoğlu Y, Aktaş B. Synthesis of Fe3O4 nanoparticles at 100 C and its magnetic characterization. J Alloys Compd. 2009;472(1-2):18-23.
33. Ibrahim M, Nada A, Kamal DE. Density functional theory and FTIR spectroscopic study of carboxyl group. Indian J Pure Appl Phys. 2005;44(12):911-7.
34. Rajabi-Moghaddam H, Naimi-Jamal MR, Tajbakhsh M. Fabrication of copper(II)-coated magnetic core-shell nanoparticles Fe_3O_4@SiO_2-2-aminobenzohydrazide and investigation of its catalytic application in the synthesis of 1,2,3-triazole compounds. Sci Rep. 2021;11(1):2073.
35. Kim DW, Kim TH, Choi S, Kim KS, Park DW. Preparation of silica coated iron oxide nanoparticles using non-transferred arc plasma. Adv Powder Technol. 2012;23(6):701-7.
36. Miri A, Najafzadeh H, Darroudi M, Miri MJ, Kouhbanani MAJ, Sarani M. Iron Oxide Nanoparticles: Biosynthesis, Magnetic Behavior, Cytotoxic Effect. ChemistryOpen. 2021;10(3):327-33.
37. Kamaly N, Farokhzad OC, Corbo C. Nanoparticle protein corona evolution: from biological impact to biomarker discovery. Nanoscale. 2022;14(5):1606-20.
38. Richtering W, Alberg I, Zentel R. Nanoparticles in the Biological Context: Surface Morphology and Protein Corona Formation. Small. 2020;16(39):e2002162.
39. Li Z, Wang Y, Zhu J, Zhang Y, Zhang W, Zhou M, et al. Emerging well-tailored nanoparticulate delivery system based on in situ regulation of the protein corona. J Control Release. 2020;320:1-18.
40. Corbo C, Molinaro R, Parodi A, Toledano Furman NE, Salvatore F, Tasciotti E. The impact of nanoparticle protein corona on cytotoxicity, immunotoxicity and target drug delivery. Nanomedicine (Lond). 2016;11(1):81-100.
41. Keshishian H, Burgess MW, Specht H, Wallace L, Clauser KR, Gillette MA, et al. Quantitative, multiplexed workflow for deep analysis of human blood plasma and biomarker discovery by mass spectrometry. Nat Protoc. 2017;12(8):1683-701.
42. Keshishian H, Burgess MW, Gillette MA, Mertins P, Clauser KR, Mani DR, et al. Multiplexed, Quantitative Workflow for Sensitive Biomarker Discovery in Plasma Yields Novel Candidates for Early Myocardial Injury. Mol Cell Proteomics. 2015;14(9):2375-93.
43. Sobsey CA, Ibrahim S, Richard VR, Gaspar V, Mitsa G, Lacasse V, et al. Targeted and Untargeted Proteomics Approaches in Biomarker Development. Proteomics. 2020;20(9):e1900029.
44. Tiambeng TN, Roberts DS, Brown KA, Zhu Y, Chen B, Wu Z, et al. Nanoproteomics enables proteoform-resolved analysis of low-abundance proteins in human serum. Nat Commun. 2020;11(1):3903.
45. Campos A, Díaz Peña R, Anschau V, You S, Motamedchaboki K, Gajadhar AS, et al. In-depth plasma proteomics profiling with nanoparticle-based Proteograph workflow: a performance evaluation of label free and TMT multiplexing approaches. 2022. Available from: https://seer.bio/wp-content/uploads/2021/11/ASMS_2021_Campos.pdf
46. Cedervall T, Lynch I, Lindman S, Berggård T, Thulin E, Nilsson H, et al. Understanding the nanoparticle-protein corona using methods to quantify exchange rates and affinities of proteins for nanoparticles. Proc Natl Acad Sci U S A. 2007;104(7):2050-5.
47. Kim YH, Kang JS. Micro-computed tomography evaluation and pathological analyses of female rats with collagen-induced arthritis. J Vet Sci. 2015;16(2):165-71.
48. Hui W, Yu D, Cao Z, Zhao X. Butyrate inhibit collagen-induced arthritis via Treg/IL-10/Th17 axis. Int Immunopharmacol. 2019;68:226-33.